Optics Letters

Compact narrow-linewidth integrated laser based on a low-loss silicon nitride ring resonator

Brian Stern,[1,2] Xingchen Ji,[1,2] Avik Dutt,[1,2] and Michal Lipson[2,*]

[1]School of Electrical and Computer Engineering, Cornell University, Ithaca, New York 14853, USA
[2]Department of Electrical Engineering, Columbia University, New York, New York 10027, USA
*Corresponding author: ml3745@columbia.edu

Received 19 September 2017; revised 8 October 2017; accepted 9 October 2017; posted 9 October 2017 (Doc. ID 307092); published 31 October 2017

We design and demonstrate a compact, narrow-linewidth integrated laser based on low-loss silicon nitride waveguides coupled to a III-V gain chip. By using a highly confined optical mode, we simultaneously achieve compact bends and ultra-low loss. We leverage the narrowband backreflection of a high-Q microring resonator to act as a cavity output mirror, a single-mode filter, and a propagation delay all in one. This configuration allows the ring to provide feedback and obtain a laser linewidth of 13 kHz with 1.7 mW output power around 1550 nm. This demonstration realizes a compact sub-millimeter silicon nitride laser cavity with a narrow linewidth.

OCIS codes: (140.0140) Lasers and laser optics; (060.4510) Optical communications; (130.0130) Integrated optics.

https://doi.org/10.1364/OL.42.004541

Narrow-linewidth lasers are critical for a wide range of applications that require either long coherence lengths or superior phase sensitivity. These include optical communications [1], sensing [2], spectroscopy [3], light detection and ranging (LIDAR) [4], quantum optics [5], and atomic clocks [6]. Optical communications is of particular interest as network capacity demands rapidly grow. In order to expand the capacity of long-haul, metro, and short-distance optical links, advanced modulation formats using coherent systems have emerged. Such formats modulate phase, in addition to amplitude, in order to increase aggregate data rates. This reliance on phase sets stricter requirements for the laser linewidth. For example, 16-state quadrature amplitude modulation (16QAM) can require linewidths below 100 kHz, and higher formats have requirements down to the single kHz level [7], far narrower than the approximately 1 MHz linewidth of typical distributed feedback (DFB) or distributed Bragg reflector (DBR) lasers.

Optical networks are moving towards integrated, chip-based solutions in order to address the size, power, and cost of optical transceivers [8,9], with most research focusing on silicon cavities. In systems integrating multiple lasers, e.g., wavelength-division multiplexing, the realization of compact lasers enables scaling and cost reduction. Integrated, tunable lasers based on silicon photonics have been demonstrated using III-V materials such as InP, which has been bonded [10,11], epitaxially grown [12], or hybridly attached [13–16] to the silicon chip. These electrically pumped lasers have achieved excellent output power, efficiency, and tuning range with linewidths reaching below 10 kHz [15].

Compact narrow-linewidth lasers based on silicon nitride (Si_3N_4)—a CMOS-compatible, deposited material with low nonlinear losses—would provide numerous advantages over silicon for many applications. In contrast to silicon, Si_3N_4 is not limited by two-photon absorption or free-carrier absorption at higher powers [17], while still having a high index contrast (∼0.5) allowing for compact devices. Additionally, its transparency extends to visible wavelengths, enabling additional applications [2,5,6]. While Si_3N_4 integrated laser cavities reaching linewidths as low as 24 kHz [18–22] have been demonstrated, they rely on mode delocalization in order to achieve low loss, requiring long lengths [18–21] or large areas (on the order of several mm^2) in order to ensure low bending losses [22].

Here we present a compact Si_3N_4 hybrid laser based on high-confinement waveguides in order to attain a low-loss, small footprint integrated laser cavity. We leverage our recently demonstrated Si_3N_4 waveguides with propagation losses as low as 0.8 dB/m at 100 μm radius [23], achieved by addressing sources of loss and confining the optical mode. Such high-confinement Si_3N_4 waveguides also compare favorably to silicon, which has only reached losses of 10–50 dB/m at compact dimensions [15,24] or 3 dB/m at 5 mm size [25].

We use a high quality factor (Q) Si_3N_4 microring resonator as a combined filter, output mirror, and propagation delay to achieve linewidth reduction. The laser consists only of a gain section and two mirrors, one of which is the high-Q microring, as shown in Fig. 1(a). The ring resonator acts as a partial reflector, as well as a tunable filter, by taking advantage of the coupling between the counter-clockwise (CCW) and the clockwise (CW) propagation modes [26,27]. Note that this effect was first used in fiber [27] and later free-space lasers [28], while we now demonstrate that it can be applied to planar resonators. The CW and CCW modes couple to each other when minor scattering points along the cavity dominate the losses, as opposed to material absorption or out-of-plane scattering. When the Q is sufficiently high, power builds in the cavity such that light

can fully couple from CW to CCW or the reverse, resulting in an effective reflection. The amount of reflection is controlled by the coupling strength between the two modes and by the Q relative to the coupling strength κ between the input waveguide and the ring [26]. Because the reflection has a narrow bandwidth, the microring also filters the cavity modes. Tuning the ring's resonance allows the lasing wavelength to be selected.

To achieve a narrow laser linewidth, we utilize the high-Q microring as external cavity feedback and take advantage of the long effective length of the ring. In semiconductor lasers, spontaneous emission events affect carrier density, resulting in refractive index and phase changes, thus broadening the linewidth [29]. An external cavity reduces this linewidth broadening by making the lasing frequency less sensitive to phase and gain changes [30]. Because frequency-dependent feedback contributes to linewidth reduction, the narrowband reflection from the ring in our design makes an ideal external cavity. The low propagation loss and coupling strength of the microring effectively increases the cavity length. The effective length L_{eff} of the ring is given by

$$L_{\text{eff}} = \frac{\lambda}{\beta}\left|\frac{d\varphi}{d\lambda}\right|, \tag{1}$$

where β is the propagation constant [31]. At critical coupling, this becomes

$$L_{\text{eff}} = \frac{1-\kappa}{\kappa}L. \tag{2}$$

To achieve a large L_{eff}, we operate close to critical coupling with low coupling κ. The L_{eff} provides the linewidth reduction benefits of a physically long external cavity, without the need for centimeters of on-chip space. Note that demonstrations using microcavities in lasers have previously achieved sub-kilohertz linewidths using feedback from MgF_2 or silica microsphere cavities with Qs on the order of 10^9 to achieve ultra-narrow resonances [32,33], but such materials are not planar and, therefore, not easily integrated on silicon substrates.

To ensure that low-loss waveguides translate to a high loaded quality factor (Q_L) and a narrow linewidth, we use a single waveguide to couple light in and out of the ring in contrast to the more commonly used add/drop configuration formed by coupling the ring to two waveguides [see Fig. 1(b), top]. In a single waveguide pass-by configuration [Fig. 1(b), bottom], the coupling κ must match the roundtrip losses αL in order to achieve critical coupling so that power builds in the ring. We operate the ring in the undercoupled regime, where κ is slightly less than αL. This leads to a high Q_L close to the intrinsic Q_0, where $Q_L = Q_0/(1+\kappa/\alpha L)$. In contrast, the commonly used add-drop ring configuration shown in Fig. 1(b) (top) must meet the condition $\kappa = \kappa' + \alpha L$ for critical coupling. In this case, the coupling ($\kappa \cong \kappa'$) must be strong compared to αL to drop the power and, thus, even a low-loss platform may be limited to a Q_L on the order of 10^5. Therefore, the pass-by configuration used here is preferred to achieve a high Q_L in the 10^7 range, which takes advantage of Si_3N_4's low loss.

We form the laser by edge coupling a III-V reflective semiconductor optical amplifier (RSOA) to the Si_3N_4 cavity [Fig. 1(c)]. The RSOA is commercially available (Thorlabs SAF1126) and provides gain across a 40 nm range near 1550 nm, for which we design the laser cavity. The RSOA has a reflection of 93% at one facet and is anti-reflection coated on the other, which is coupled to a tapered Si_3N_4 waveguide. The taper is fabricated at an angle with respect to the facet to avoid reflections. We use a three-axis stage to align the RSOA to the silicon chip facet [Fig. 2(a)] and estimate a coupling loss of 8.5 dB. This can be improved by reducing the separation in air between the two chips to avoid diffraction, as coupling loss below 1 dB has recently been demonstrated in hybrid lasers [15]. The Si_3N_4 waveguide has a length of 950 μm before coupling to a 120 μm radius microring resonator. We use a coupling gap of 480 nm and wide waveguides with a cross section of 730 nm × 1800 nm to localize the optical mode. The output

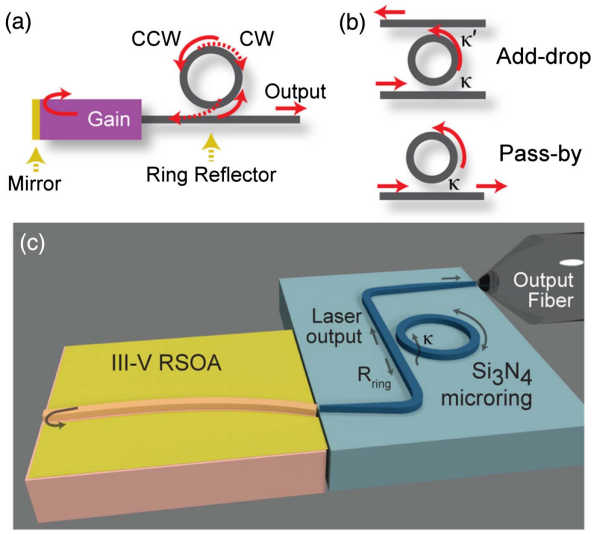

Fig. 1. (a) Schematic of our laser. The ring acts as a partial reflector by taking advantage of the coupling of the CCW propagating mode to the CW mode, which reflects light back into the cavity. (b) Comparison of the pass-by configuration used here (bottom), which leads to a high loaded Q, with the commonly used add-drop configuration (top), which often leads to a lower loaded Q. (c) Schematic of our laser cavity design (not to scale).

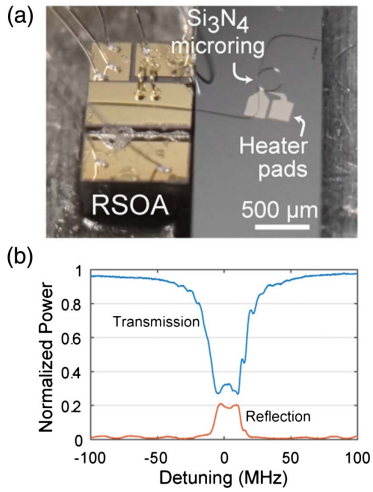

Fig. 2. (a) Photograph of the coupled chips. Wire bonds are used to supply current to the RSOA, and needle probes (not shown) are used to apply voltage to the heater on the Si_3N_4 chip. (b) Measured transmission and reflection spectra of a Si_3N_4 microring resonator. The degeneracy of the CW and CCW modes causes the resonance splitting (double peak), which is accounted for in the resonance fitting.

waveguide is then coupled to a lensed fiber to measure the output of the laser.

We fabricate the Si_3N_4 cavity using the process described in Ref. [23] to attain low loss waveguides. We grow 4 μm of SiO_2 on a silicon wafer and then deposit Si_3N_4 using low-pressure chemical vapor deposition. The wafer is annealed to remove hydrogen impurities. We then pattern the waveguides using electron beam lithography; next, we etch the waveguides and clad the devices with SiO_2. Finally, we pattern and lift off sputtered platinum heaters over the microring in order to tune the resonance.

We measure the quality factor of the Si_3N_4 microring to be over 10^7 which, in the laser configuration, corresponds to an effective length of over 1 m. Using the measurements of the transmission of the Si_3N_4 chip alone, shown in Fig. 2(b), we fit the microring resonance bandwidth to an 18 MHz Lorentzian, indicating a Q_0 of 1.34×10^7, a Q_L of 1.05×10^7, and an ultra-low propagation loss of 2.2 dB/m. We use a circulator to measure the reflection spectrum of the microring, which is shown in Fig. 2(b). On resonance, there is a strong 20% reflection. Using the Q_L derived from the transmission, we determine κ to be 1.1×10^{-4}. From Eq. (1) and the transmission fitting, L_{eff} is calculated to be 1.17 m, achieved in an area of about 4.5×10^{-2} mm^2 on the chip.

We observe single-mode lasing and greater than 1 mW of output power when pumping the assembled laser above threshold. The output of the laser is sent to an optical spectrum analyzer (OSA) to characterize the lasing spectrum, shown in Fig. 3(a). The laser's side-mode suppression ratio (SMSR) is 41 dB at 1550 nm. Figure 3(b) shows the laser's output power versus the pump current. The threshold current is 52 mA, above which the slope efficiency is 48 mW/A. The laser, which is uncooled, has a maximum observed output power of 1.66 mW at 90 mA, with a wall-plug efficiency of 1.7%. In order to confirm that the ring is acting as an output mirror according to design, we also couple the RSOA to an identical Si_3N_4 waveguide, but with no on-chip ring, and confirm that it does not lase simply due to facet reflections. Figure 3(c) shows that as we tune the resonance of the ring using the integrated heaters, we observe lasing at wavelengths from 1544 to 1571 nm, a wide 27 nm range, although the tuning, while repeatable, does not continuously cover the whole tuning range.

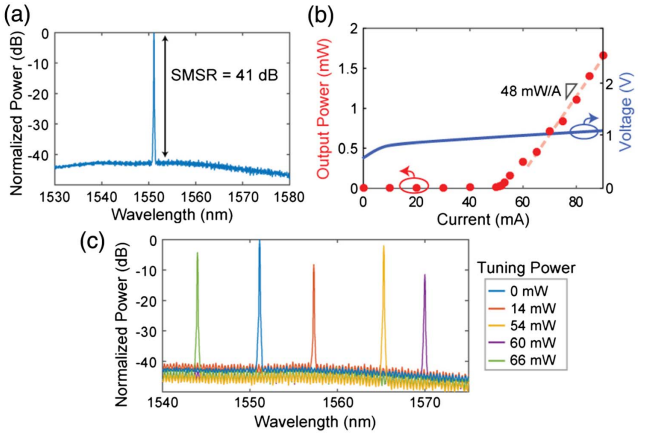

Fig. 3. (a) Measured spectrum of laser output showing single-mode operation and high SMSR. (b) Measured uncooled laser output power at room temperature. (c) Measured spectra showing lasing across a wide range of wavelengths. By adjusting the voltage applied to the micro-heater integrated on the ring, lasing is obtained at discrete wavelengths within a 27 nm range.

We measure a 13 kHz linewidth from the laser using a delayed self-heterodyne (DSH) setup. The linewidth is narrower than the resolution of our OSA, so we perform DSH because it allows measurement of narrow linewidths without the need for a reference laser at a nearby frequency [34]. Figure 4(a) shows our experimental setup. We send the laser output to a fiber interferometer in which one path has a delay of 12 km, which is longer than the laser coherence length and allows reliable measurements for linewidths down to several kilohertz. To further improve the confidence of our setup, we also independently measured the linewidth of a commercial laser and verified it to be equal to the specified 2.4 kHz linewidth. Figure 4(b) shows the measured beat note of our integrated laser using this setup. We fit a Lorentzian to the beat note's tails, corresponding to a linewidth of 13 kHz, which is among the narrowest demonstrated in integrated lasers with widely adjustable wavelengths.

According to our analysis, a linewidth as narrow as 400 Hz should be achievable if we overcome technical noise, and even narrower linewidths are possible with reasonable improvements to the Q and the coupling loss between the RSOA and chip. Using the experimentally demonstrated cavity parameters, we plot the predicted linewidth as a function of Q_L in Fig. 5, using the Schawlow–Townes formula with Henry's linewidth broadening factor [29]. For the Q_L of 1.05×10^7, in our case, the expected linewidth is 400 Hz, indicating that in our experiment we are likely limited by technical noise, such as vibrations or noise from the power supply driving the RSOA. Permanent bonding of the two chips or using a lower noise pump current supply could help reach this prediction. We also plot in Fig. 5 the achievable linewidths from optimized coupling of the gain chip to the silicon chip, which we assume can improve to 1 dB loss [15] and 10 mW output power. We see that this optimization is expected to yield a linewidth of 20 Hz for the same Q_L, and below 1 Hz for a Q_L of 5.8×10^7. This Q_L was achieved in Si_3N_4 in Ref. [23]. Such ultra-narrow linewidths would be especially desirable for metrology applications. It is important to note that at these levels, factors such as acoustic noise and Brownian motion may also become limiting factors [33], but using a fully integrated platform aids one in addressing these challenges.

In summary, we have demonstrated a compact Si_3N_4 laser cavity with a narrow linewidth. Using a highly confined optical

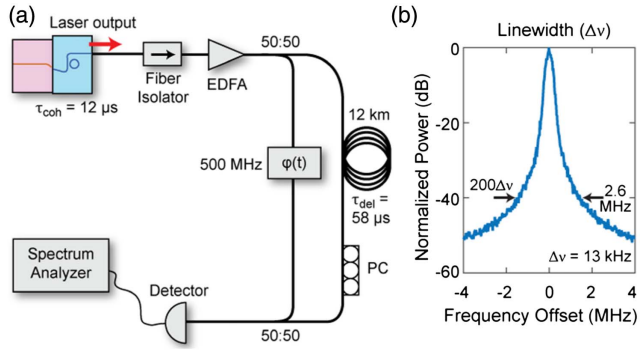

Fig. 4. (a) DSH test setup. EDFA, erbium-doped fiber amplifier; PC, polarization controller. (b) Measured DSH beat note in radio frequency (RF) spectrum analyzer. The −40 dB width equals 200 times the Lorentzian linewidth, which is found to be 13 kHz here. The resolution bandwidth used is 10 kHz with a 325 ms sweep time.

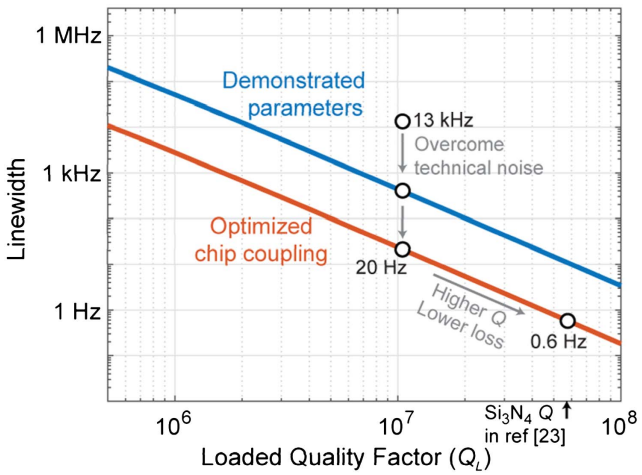

Fig. 5. Calculated linewidth versus Q, with current cavity parameters (blue) and improved coupling (red). Laser cavities based on Si_3N_4 have the potential to reach beyond the demonstrated 13 kHz linewidth and produce sub-hertz linewidths.

mode enables both compact bends and ultra-low loss in Si_3N_4 waveguides. Our design leverages the narrowband reflection generated by backscattering in a high-Q Si_3N_4 microring to act as an output mirror and to provide laser linewidth reduction. The narrow resonance of the ring allows the laser to achieve single-mode lasing with a 41 dB SMSR. We have shown lasing at discrete wavelengths across a 27 nm range. A larger continuous tuning range should be possible with additional cavity control that would include a tunable coarse filter. Further, an additional heater to tune the cavity phase would allow for more consistent output power while tuning. The laser has a measured 13 kHz linewidth, due to a high-Q of over 10^7 and a low κ coupling design which results in an effective length of over 1 m in a sub-millimeter area. In addition to the C-band (1550 nm) laser demonstrated here, a design using amplifiers at 1310 nm or, even visible wavelengths, would also be possible due to Si_3N_4's broad transparency. Approaches using heterogeneous bonding [10,11], rather than edge coupling, should be compatible with this novel cavity architecture as well. Further enhancements in cavity parameters could enable sub-hertz linewidths on a Si_3N_4 platform, which may otherwise be far beyond the reach of silicon.

Funding. Defense Advanced Research Project Administration (DARPA) (HR0011-16-C-0107); National Science Foundation (NSF) (ECCS-1542081).

Acknowledgment. The work in this Letter was performed in part at the Cornell NanoScale Facility.

REFERENCES

1. B. J. Puttnam, R. S. Luís, W. Klaus, J. Sakaguchi, J. M. D. Mendinueta, Y. Awaji, N. Wada, Y. Tamura, T. Hayashi, M. Hirano, and J. Marciante, in *European Conference on Optical Communication (ECOC)* (2015), pp. 1–3.
2. I. M. White, H. Zhu, J. D. Suter, N. M. Hanumegowda, H. Oveys, M. Zourob, and X. Fan, IEEE Sens. J. **7**, 28 (2007).
3. W.-C. Lai, S. Chakravarty, X. Wang, C. Lin, and R. T. Chen, Appl. Phys. Lett. **98**, 023304 (2011).
4. E. Dale, W. Liang, D. Eliyahu, A. Savchenkov, V. Ilchenko, A. B. Matsko, D. Seidel, and L. Maleki, *Imaging and Applied Optics* (Optical Society of America, 2014), paper JTu2C.3.
5. N. Prtljaga, C. Bentham, J. O'Hara, B. Royall, E. Clarke, L. R. Wilson, M. S. Skolnick, and A. M. Fox, Appl. Phys. Lett. **108**, 251101 (2016).
6. B. J. Bloom, T. L. Nicholson, J. R. Williams, S. L. Campbell, M. Bishof, X. Zhang, W. Zhang, S. L. Bromley, and J. Ye, Nature **506**, 71 (2014).
7. M. Seimetz, *Conference on Optical Fiber communication/National Fiber Optic Engineers Conference (OFC/NFOEC)* (2008), pp. 1–3.
8. C. R. Doerr, L. Chen, D. Vermeulen, T. Nielsen, S. Azemati, S. Stulz, G. McBrien, X.-M. Xu, B. Mikkelsen, M. Givehchi, C. Rasmussen, and S. Y. Park, in *Optical Fiber Communication Conference: Postdeadline Papers* (Optical Society of America, 2014), paper Th5C.1.
9. P. Dong, X. Liu, S. Chandrasekhar, L. L. Buhl, R. Aroca, and Y. K. Chen, IEEE J. Sel. Top. Quantum Electron. **20**, 150 (2014).
10. Y. de Koninck, G. Roelkens, and R. Baets, IEEE Photon. J. **5**, 2700413 (2013).
11. T. Komljenovic, S. Srinivasan, E. Norberg, M. Davenport, G. Fish, and J. E. Bowers, IEEE J. Sel. Top. Quantum Electron. **21**, 214 (2015).
12. Z. Wang, B. Tian, M. Pantouvaki, W. Guo, P. Absil, J. Van Campenhout, C. Merckling, and D. Van Thourhout, Nat. Photonics **9**, 837 (2015).
13. N. Fujioka, T. Chu, and M. Ishizaka, J. Lightwave Technol. **28**, 3115 (2010).
14. J.-H. Lee, J. Bovington, I. Shubin, Y. Luo, J. Yao, S. Lin, J. E. Cunningham, K. Raj, A. V. Krishnamoorthy, and X. Zheng, Opt. Express **23**, 12079 (2015).
15. N. Kobayashi, K. Sato, M. Namiwaka, K. Yamamoto, S. Watanabe, T. Kita, H. Yamada, and H. Yamazaki, J. Lightwave Technol. **33**, 1241 (2015).
16. S. Yang, Y. Zhang, D. W. Grund, G. A. Ejzak, Y. Liu, A. Novack, D. Prather, A. E.-J. Lim, G.-Q. Lo, T. Baehr-Jones, and M. Hochberg, Opt. Express **22**, 1172 (2014).
17. D. T. H. Tan, K. Ikeda, P. C. Sun, and Y. Fainman, Appl. Phys. Lett. **96**, 061101 (2010).
18. R. M. Oldenbeuving, E. J. Klein, H. L. Offerhaus, C. J. Lee, H. Song, and K.-J. Boller, Laser Phys. Lett. **10**, 015804 (2013).
19. Y. Fan, R. M. Oldenbeuving, E. J. Klein, C. J. Lee, H. Song, M. R. H. Khan, H. L. Offerhaus, P. J. M. van der Slot, and K.-J. Boller, Proc. SPIE **9135**, 91351B (2014).
20. J. L. Zhao, R. M. Oldenbeuving, J. P. Epping, M. Hoekman, R. G. Heideman, R. Dekker, Y. Fan, K. J. Boller, R. Q. Ji, S. M. Fu, and L. Zeng, in *2016 IEEE 13th International Conference on Group IV Photonics (GFP)* (2016), pp. 24–25.
21. Y. Fan, J. P. Epping, R. M. Oldenbeuving, C. G. H. Roeloffzen, M. Hoekman, R. Dekker, R. G. Heideman, P. J. M. van der Slot, and K. J. Boller, IEEE Photon. J. **8**, 1505111 (2016).
22. D. T. Spencer, M. L. Davenport, T. Komljenovic, S. Srinivasan, and J. E. Bowers, Opt. Express **24**, 13511 (2016).
23. X. Ji, F. A. S. Barbosa, S. P. Roberts, A. Dutt, J. Cardenas, Y. Okawachi, A. Bryant, A. L. Gaeta, and M. Lipson, Optica **4**, 619 (2017).
24. M. Borselli, T. J. Johnson, and O. Painter, Opt. Express **13**, 1515 (2005).
25. A. Biberman, M. J. Shaw, E. Timurdogan, J. B. Wright, and M. R. Watts, Opt. Lett. **37**, 4236 (2012).
26. T. J. Kippenberg, S. M. Spillane, and K. J. Vahala, Opt. Lett. **27**, 1669 (2002).
27. K. Kieu and M. Mansuripur, Opt. Lett. **32**, 244 (2007).
28. Z. Xie, W. Liang, A. A. Savchenkov, J. Lim, J. Burkhart, M. McDonald, T. Zelevinsky, V. S. Ilchenko, A. B. Matsko, L. Maleki, and C. W. Wong, Opt. Lett. **40**, 2596 (2015).
29. C. Henry, IEEE J. Quantum Electron. **18**, 259 (1982).
30. R. Kazarinov and C. Henry, IEEE J. Quantum Electron. **23**, 1401 (1987).
31. B. Liu, A. Shakouri, and J. E. Bowers, Appl. Phys. Lett. **79**, 3561 (2001).
32. W. Liang, V. S. Ilchenko, A. A. Savchenkov, A. B. Matsko, D. Seidel, and L. Maleki, Opt. Lett. **35**, 2822 (2010).
33. J. Lim, A. A. Savchenkov, E. Dale, W. Liang, D. Eliyahu, V. Ilchenko, A. B. Matsko, L. Maleki, and C. W. Wong, Nat. Commun. **8**, 8 (2017).
34. T. Okoshi, K. Kikuchi, and A. Nakayama, Electron. Lett. **16**, 630 (1980).